

TAUP 2369-96  
September 25, 1996

## Separation of $\gamma/\pi^0$ Showers at High Energies

**J. Grunhaus and S. Kananov**

School of Physics and Astronomy, Raymond and Beverly  
Sackler Faculty of Exact Sciences, Tel Aviv University,  
Tel Aviv 69978, ISRAEL

*Submitted to Nuclear Instruments and Methods.*

### Abstract

We have designed and carried out simulation studies of a two layer Shower Maximum Detector diagonally off-set (SMD-dos) optimized for the separation of  $\pi^0$  showers from  $\gamma$  showers in the 30 to 150 GeV energy range. For 90%  $\gamma$  acceptance the SMD-dos yields  $\pi^0$  rejection efficiencies of  $92\pm 4\%$ ,  $87\pm 4\%$  and  $32\pm 2\%$ , respectively, for 30, 50 and 150 GeV incident energies. We find that the SMD-dos is superior to a conventional geometry single-layer or multiple-layer shower maximum detector (SMD), of equal granularity, by an average factor of  $\sim 1.5$  over the 50 to 150 GeV energy range. We also find that the SMD-dos gives better  $\pi^0$  rejection, for the same number of channels, than a SMD. At hadron-hadron colliders the signature of choice for the detection of the Higgs particle, in the mass range of 120 to 160 GeV, is via the decay  $H \rightarrow \gamma\gamma$ . The addition of a SMD-dos to the planned detectors at the LHC would significantly reduce the background to the  $\gamma$  signal coming from prolific  $\pi^0$  production.

# 1 Introduction

The challenging task of separating  $\pi^0$  initiated showers from  $\gamma$  initiated showers, at high incident energies, has over the past few years attracted a lot of interest and motivated extensive R and D work [1, 2, 3, 4, 5, 6, 7]. The scheduled building of the LHC machine has added new interest on the  $\gamma/\pi^0$  separation problem. The main motivation for building the LHC machine is the quest for the Higgs particle. The Standard Model has weathered extremely well strenuous experimental scrutiny during the past decades; however, it still lacks experimental support for the predicted mass generating Higgs mechanism. The only viable explanation of the masses of the elementary particles in the framework of the Standard Model is the Higgs mechanism. The two main collaborations approved for operation at the LHC, ATLAS [8] and CMS[9] state in their Technical Reports the paramount importance of the searches for the Higgs particle at the LHC machine. The upgrading of LEP to LEP2 will allow the search for the Higgs particle up to a mass of about 100 GeV. Searches for the Higgs particle at higher masses will have to wait for the operation of the LHC machine.

At hadron - hadron colliders the signature of choice for the detection of the Higgs particle, in the mass range of 120 to 160 GeV, is via the decay  $H \rightarrow \gamma\gamma$  [10]. These searches will encounter high  $\gamma$  backgrounds coming from prolific  $\pi^0$  production which decay into two  $\gamma$ 's. The attainment of good  $\pi^0/\gamma$  separation is of crucial importance to the success of the proposed searches. The incorporation of a SMD-dos into the planned detectors at the LHC would appreciably reduce the  $\gamma$  background.

We have designed and carried out simulation studies of a two layer Shower Maximum Detector diagonally off-set (SMD-dos) optimized for the separation of  $\pi^0$  showers from  $\gamma$  showers in the 30 to 150 GeV energy range. A comparison of the SMD-dos with a conventional geometry single-layer and multiple-layer shower maximum detector (SMD), having the same granularity, shows that the SMD-dos yields higher  $\pi^0$  rejection efficiency in the energy range studied.

The electromagnetic showers were generated and studied using the Monte Carlo program GEANT 3.15 implementing a 100 KeV cut for  $\gamma$ 's and electrons. The shower maximum detector, either a SMD-dos or a SMD, was embedded inside an E.M. calorimeter, consisting of a mixture of Pb and scintillator (CH) corresponding to a radiation length of 0.8 cm. The perfor-

mance of the SMD-dos was optimized by carrying out extensive Monte Carlo studies of the  $\gamma/\pi^0$  separation efficiency as a function of the following design parameters: number of scintillator layers, thickness of scintillator layer, granularity (cell size) and position of the SMD-dos or SMD inside the E.M. calorimeter. Typically, samples of 500 showers were generated for each configuration of design parameters and incident energy. The distance of the E.M. calorimeter from the interaction region was kept fixed at 150 cm, the design distance of the CMS detector approved to operate at the LHC machine, and the showers were generated so that the shower initiating particle, a  $\gamma$  or  $\pi^0$  is normally incident on the E.M. calorimeter. We have studied the stand-alone capabilities of the SMD-dos; however, since the algorithms developed assume that the energy of the shower, in question, is known, the SMD-dos must be used with an E.M. calorimeter to determine the total energy of the shower.

## 2 The Geometry of the Diagonally Off-set Shower Maximum Detector

The geometry of the SMD-dos, shown in Figure 1, consists of 2 identical scintillator layers, placed one behind the other. Each layer is subdivided into square cells which are individually read out and the energy deposited in each cell is recorded. The 2 layers are diagonally off-set with respect to each other by half a cell, so that the intersection of any four adjacent cells in one layer corresponds to the center of a cell in the other layer. Studies of the  $\gamma/\pi^0$  separation efficiency of granular detectors show that the separation efficiency decreases as a function of the distance of the shower center from the nearest intersection. Hence increasing the number of intersections per unit area enhances the separation efficiency. The area of each cell, in the front layer, overlaps symmetrically one quarter of the area of each of four adjacent cells in the back layer. And likewise the area of each cell, in the back layer, overlaps symmetrically one quarter of the area of each of four adjacent cells in the front layer. Therefore, the energy collected by a particular cell is subdivided unto 4 cells giving a substantial increase in granularity

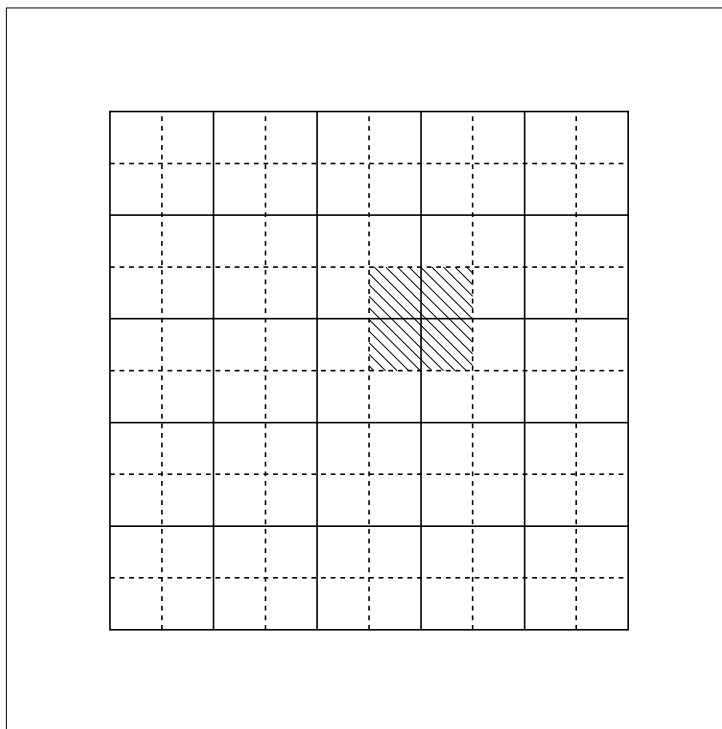


Figure 1: Layout of the two layers of the SMD-dos. The cells of the front layer are shown in solid lines and the cells of the back layer are shown in dashed lines. One back layer cell is highlighted to show the four quarter cells in the front layer which overlap it.

In the singular case that all the energy deposited by a shower is confined, in a particular layer, to one cell it is impossible with a conventional one-layer or multiple-layer SMD to determine whether the shower was initiated by a  $\gamma$  or  $\pi^0$ . However, the unique geometry of the SMD-dos, which subdivides the energy collected by a particular cell, in one layer, unto four cells in the other layer, does furnish some degree of  $\gamma/\pi^0$  separation efficiency even in this singular case.

### 3 Definition of Variables Used in the Algorithms

The energy and position information collected, per event, by the scintillator cells is used to construct 10 variables.

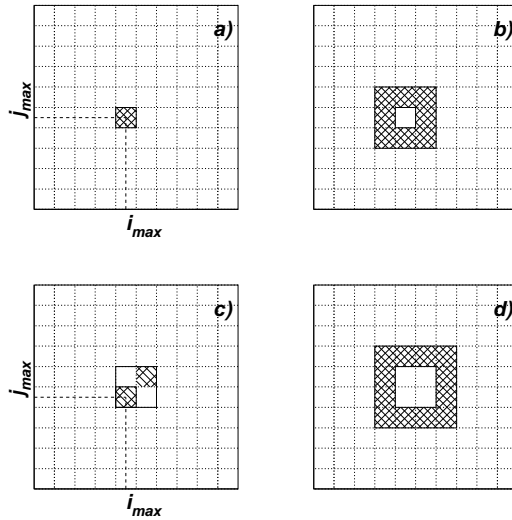


Figure 2: Display of cell configurations used in the determination of  $E_{max}$ ,  $E_4$ ,  $E_8$  and  $E_{12}$ .

These variables embody the experimental information which goes into the  $\gamma/\pi^0$  separation algorithms. The information collected in the first layer is used to construct 5 variables and likewise the information from the second layer is used to construct the other 5 variables. The detailed description and construction of these 10 variables is detailed in this section. In Figure 2 are displayed the cell configurations used for the determination of  $E_{max}$ ,  $E_4$ ,  $E_8$  and  $E_{12}$ .

- $\langle r \rangle$ , the average energy weighted radius of the shower. The determination of  $\langle r \rangle$  from the data collected by the cells in the layer is discussed in the following paragraph.

- $E_{max}$ , the maximum energy deposited in a single cell, in the layer. See Fig. 2a.
- $E_8$ , the sum of energies deposited in the eight cells which surround the cell with the maximum energy.  $E_8$  is normalized to  $E_{total}$ . See Fig. 2b.
- $E_4$ , the sum of energies deposited in a 4 cell square which includes the cells with the maximum and next to maximum energy.  $E_4$  is normalized to  $E_{total}$ . See Fig. 2c.
- $E_{12}$ , the sum of energies deposited in the 12 cells which surround the 4 cell square described in the preceding item.  $E_{12}$  is normalized to  $E_{total}$ . See Fig. 2d.

The energy information gathered by each cell is read out separately and is labelled,  $E_{ij}$ , where the x and y coordinates of the particular cell, in the two dimensional layer, are denoted, respectively, by the  $i$  and  $j$  subscripts. The average energy weighted radius,  $\langle r \rangle$ , is calculated for each layer separately. First the coordinates of the energy weighted center of the shower,  $x_0$  and  $y_0$ , are calculated as follows:  $x_0 = \sum_{i,j} E_{ij}x_i / \sum_{i,j} E_{ij}$  and  $y_0 = \sum_{i,j} E_{ij}y_i / \sum_{i,j} E_{ij}$ , where the  $i$  and  $j$  summations are carried out over all the cells that have collected energy and for  $i < j$ , to avoid double counting. Using the  $x_0$  and  $y_0$  values, we determine the distances  $r_{ij}$  between the center of the  $ij$  cell and the shower energy weighted center,  $r_{ij} = \sqrt{(x_0 - x_i)^2 + (y_0 - y_j)^2}$ . The average energy weighted radius of the shower,  $\langle r \rangle$ , is determined as follows:

$$\langle r \rangle = \frac{\sum_{i,j} E_{ij}r_{ij}}{\sum_{i,j} E_{ij}}.$$

Information, per event, from both layers is used to construct the 2 layer correlation variables. In the following we differentiate between the data gathered in the layer that recorded the cell with the maximum energy, the *leading* layer, and label them with the superscript,  $l$ , and the data from the other layer, the *non-leading* layer, and label them with the superscript,  $n$ .

The following 6 variables embody the 2 layer correlation information used in the algorithms: the correlations between  $E_{max}$  from one layer and  $E_4$  from the other layer are contained in the variables  $C_1$  and  $C_2$ . Similarly, the

correlations between  $E_4$  and  $E_8$  are contained in the variables  $C_3$  and  $C_4$  and, finally, the correlations between  $E_8$  and  $E_{12}$  are contained in  $C_5$  and  $C_6$ .

- $C_1$  is the difference,  $E_4^n - E_{max}^l$ , normalized to  $E_{total}$ .
- $C_2$  is the difference,  $E_4^l - E_{max}^n$ , normalized to  $E_{total}$ . Notice that  $C_2$  is similar to  $C_1$  with the roles of the 2 layers interchanged.
- $C_3$  is the difference  $E_4^n - E_8^l$  normalized to  $E_{total}$ .
- $C_4$  is the difference  $E_4^l - E_8^n$  normalized to  $E_{total}$ .  $C_4$  is similar to  $C_3$  with the roles of the 2 layers interchanged.
- $C_5$  is the difference  $E_8^n - E_{12}^l$  normalized to  $E_{total}$ .
- $C_6$  is the difference  $E_8^l - E_{12}^n$  normalized to  $E_{total}$ .  $C_6$  is similar to  $C_5$  with the roles of the 2 layers interchanged.

## 4 Analysis

The study of the separation of  $\gamma/\pi^0$  showers is quantified by determining the rejection efficiency of  $\pi^0$  initiated showers as a function of the acceptance of  $\gamma$  initiated showers. Eight variables are used in these analyses: the six correlations,  $C_1, \dots, C_6$  and the two average energy weighted radii,  $\langle r \rangle^l$  and  $\langle r \rangle^n$ .

For every configuration of design parameters and incident energy studied, two samples of showers, one initiated by  $\gamma$ 's and the other by  $\pi^0$ 's, were generated and propagated through the E.M. calorimeter and the SMD-dos. The shower information collected by the SMD-dos was used to construct the 8 variables previously described. A program which uses the Simulated Annealing Algorithm was utilized to delineate an 8-dimensional volume, corresponding to the 8 variables used, which contains a fixed percentage of the  $\gamma$  initiated showers while keeping to a minimum the number of  $\pi^0$  initiated showers. The delineation of this volume sets upper or lower cutoff values for each of the 8 variables. The  $\pi^0$  rejection efficiency is equal to the percentage of  $\pi^0$  initiated showers which are excluded from the delineated 8-dimensional volume.

The shower information collected by the SMD was also processed using the same analysis chain detailed above. However, since for the SMD no correlation information is available, the following variables were used:  $E_4$ ,  $E_8$ ,  $E_{12}$  and  $\langle r \rangle$ .

The computer flow chart of the program used along with a short description of those aspects of the program which are specific to the  $\gamma/\pi^0$  separation problem can be found elsewhere [4]. In Fig. 3 are shown the projections, for 50 and 100 GeV, of the 8-dimensional volume of  $\gamma$  initiated showers and  $\pi^0$  initiated showers, separately, unto the plane spanned by the correlation variables  $C_1$  and  $C_3$ .

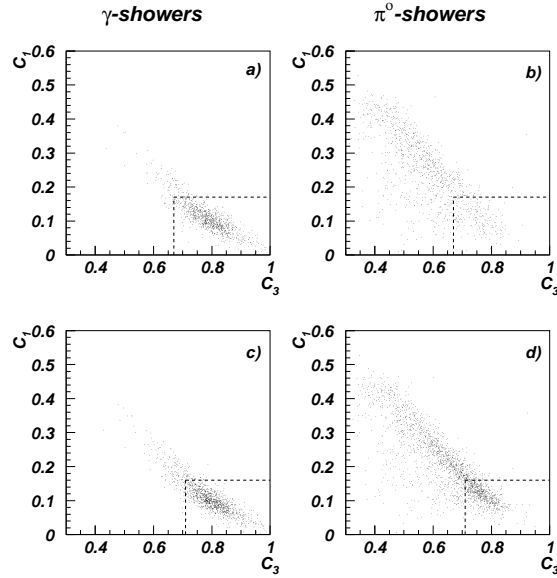


Figure 3: Scatterplots of the correlation variables  $C_3$  versus  $C_1$  for showers initiated by  $\gamma$ 's and  $\pi^0$ 's. a) 50 GeV  $\gamma$  showers and b) 50 GeV  $\pi^0$  showers. c) 100 GeV  $\gamma$  showers and d) 100 GeV  $\pi^0$  showers. The respective cutoff values of  $C_1$  and  $C_3$ , for 90%  $\gamma$  acceptance, at 50 GeV and 100 GeV, are shown by dashed rectangles on the lower right corner of each figure.

The cutoff values of  $C_1$  and  $C_3$  for 90% acceptance of the  $\gamma$  initiated showers define the rectangles shown in the lower right corners. For 50 GeV incident energy the  $\pi^0$  initiated showers overwhelmingly fall outside the ac-

ceptance rectangle giving high  $\pi^0$  rejection efficiency while for 100 GeV incident energy the number of  $\pi^0$  initiated showers excluded from the acceptance rectangle is smaller hence giving lower  $\pi^0$  rejection efficiency .

The cutoff values for different incident energies are given in Table 1. These cutoff values as well as all other results presented in this paper, for the SMD-dos and SMD, were determined from samples of 500 showers each which were generated under the following conditions:

- The distance of the E.M. calorimeter from the interaction region was fixed at 150 cm.
- The shower initiating particle,  $\gamma$  or  $\pi^0$ , was incident normally on the E.M. calorimeter. However, the direction of the initiating particle was spread randomly within a small angular range corresponding to an area of a few cells of the SMD-dos or SMD.
- The  $\pi^0$  rejection efficiency was calculated for 90%  $\gamma$  acceptance.
- The SMD-dos or SMD was positioned at a depth of 6  $X_0$ 's inside the E.M. calorimeter.
- Thickness of the scintillator layers set at 4 mm.
- The nominal granularity, cell size, is  $1 \times 1 \text{ cm}^2$ . In the event that a different cell size was used, it is explicitly stated.

$E_{in}$	$C_1 \leq$	$C_2 \leq$	$C_3 \geq$	$C_4 \geq$	$C_5 \leq$	$C_6 \leq$	$\langle r \rangle^l \leq$	$\langle r \rangle^n \leq$
30	0.18	0.70	0.65	0.21	0.65	0.17	0.58	0.80
50	0.17	0.65	0.67	0.22	0.63	0.15	0.55	0.82
80	0.17	0.68	0.70	0.20	0.62	0.16	0.53	0.85
100	0.16	0.70	0.71	0.22	0.65	0.18	0.50	0.88
120	0.15	0.67	0.71	0.23	0.60	0.14	0.50	0.90
150	0.15	0.64	0.73	0.23	0.58	0.15	0.48	0.91

Table 1: Cutoff values of the six correlation variables,  $C_1, \dots, C_6$ , and the two average energy weighted radii,  $\langle r \rangle^l$  and  $\langle r \rangle^n$ , for incident energies of 30 to 150 GeV.

## 5 Results and Discussion

The  $\pi^0$  rejection efficiency as a function of the incident energy of the showering particle is shown in Fig. 4a for both the SMD-dos and SMD. Both detectors have equal granularity,  $1 \times 1 \text{ cm}^2$  cells. The  $\pi^0$  rejection efficiency of the SMD-dos and the SMD decrease as a function of energy; however, the  $\pi^0$  rejection efficiency of the SMD-dos is higher than that of the SMD over the whole energy range. The ratio of the rejection efficiency of the SMD-dos to the SMD, the ‘advantage factor’, is plotted as function of energy in Fig. 4b.

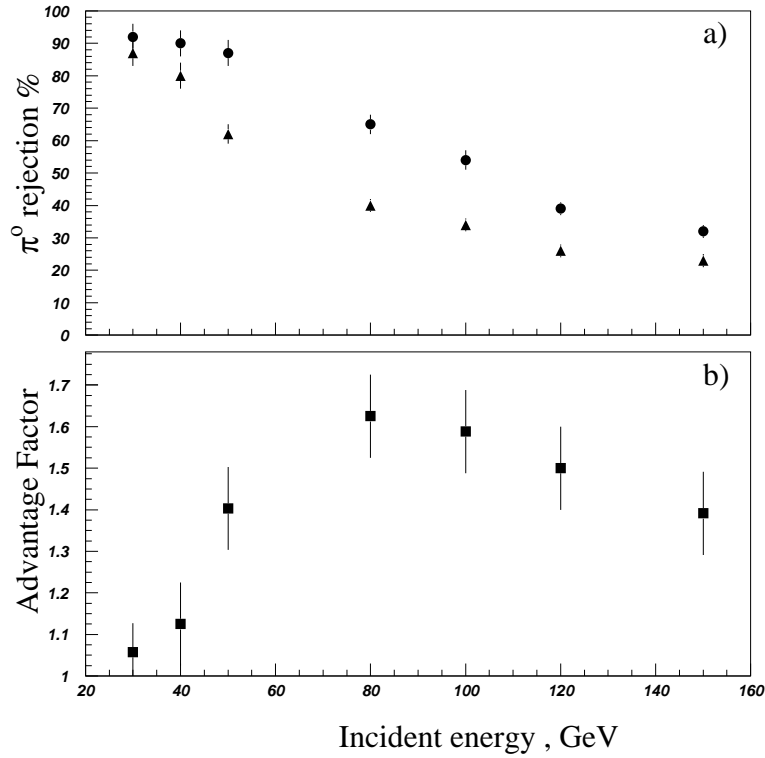


Figure 4: a) The  $\pi^0$  rejection efficiency of the SMD-dos ( $\bullet$ ) and a conventional SMD ( $\blacktriangle$ ) as a function of incident energy. b) The ‘advantage factor’ ( $\blacksquare$ ) of the SMD-dos over the SMD as a function of incident energy.

The value of the ‘advantage factor’ is close to 1.0 at 30 GeV and it then rises to a maximum value of 1.63 at 80 GeV. With increasing energy the value of the ‘advantage factor’ decreases gradually reaching the value of 1.39 at 150 GeV, the highest energy studied. In Table 2 are summarized the the  $\pi^0$  rejection efficiencies of the SMD-dos and SMD, of equal granularity, for various incident energies. The ‘advantage factor’ has been calculated for each incident energy. The following parameters, which are relevant to  $\gamma/\pi^0$  separation problems are given, per energy, in Table 2:  $\Theta_{12}$ , the minimum opening angle in the lab system of the  $\pi^0 \rightarrow \gamma\gamma$  decay;  $d_{1,2}$ , the distance between the two  $\gamma$  centers at the position of the SMD-dos or SMD and the ratio  $d_{1,2}/\Delta$ , where  $\Delta$  is the length of cell side, 1 cm.

$E_{in}$ [GeV]	$\pi^0$ Rejection SMD-dos [%]	$\Theta_{12}$ [mrad]	$d_{1,2}$ [cm]	$\frac{d_{1,2}}{\Delta}$	$\pi^0$ Rejection SMD [%]	‘advantage factor’
30	92±4	9.3	1.43	1.43	87±4	1.06±0.07
40	90±4	7.0	1.07	1.07	80±4	1.13±0.08
50	87±4	5.6	0.86	0.86	62±3	1.40±0.09
80	65±3	3.5	0.55	0.55	40±2	1.63±0.11
100	54±3	2.8	0.43	0.43	34±2	1.59±0.13
120	39±2	2.3	0.36	0.36	26±2	1.50±0.14
150	32±2	1.9	0.29	0.29	23±2	1.39±0.14

Table 2: The  $\pi^0$  rejection efficiency of the SMD-dos and SMD, of equal granularity, is presented for different values of incident energy. The following parameters, which are explained in the text, are given per incident energy:  $\Theta_{12}$ ,  $d_{1,2}$ , the ratio  $d_{1,2}/\Delta$  and the ‘advantage factor’.

Results of studies of the dependence of the  $\pi^0$  rejection efficiencies of the SMD-dos and SMD on the detector granularity, which were done for 50 and 100 GeV incident energies, are shown in Figure 5 and summarized in Table 3. The expected increase in  $\pi^0$  rejection efficiency with increasing detector granularity for both SMD-dos and SMD is seen in Fig. 5a.

For 50 GeV incident energy the  $\pi^0$  rejection efficiency of the of the SMD-dos and the SMD converge as the granularity increases. The ‘advantage factor’, plotted in Fig. 5b, is seen to fall rapidly from a value of 1.71 for granularity of  $7 \times 7$  to a value of 1.09 for a granularity of  $14 \times 14$ . The ‘advantage factor’ for granularity of  $20 \times 20$  is consistent with 1.0. For 100

GeV incident energy the  $\pi^0$  rejection efficiency of both the SMD-dos and the SMD increase with increasing granularity; however, the  $\pi^0$  rejection efficiency of the SMD-dos is higher over the whole energy range. The 'advantage factor' has a value of 1.4 at  $7 \times 7$  granularity, it attains the maximum value of 1.7 at granularity of  $14 \times 14$  and it then decreases to 1.5 for  $20 \times 20$  granularity.

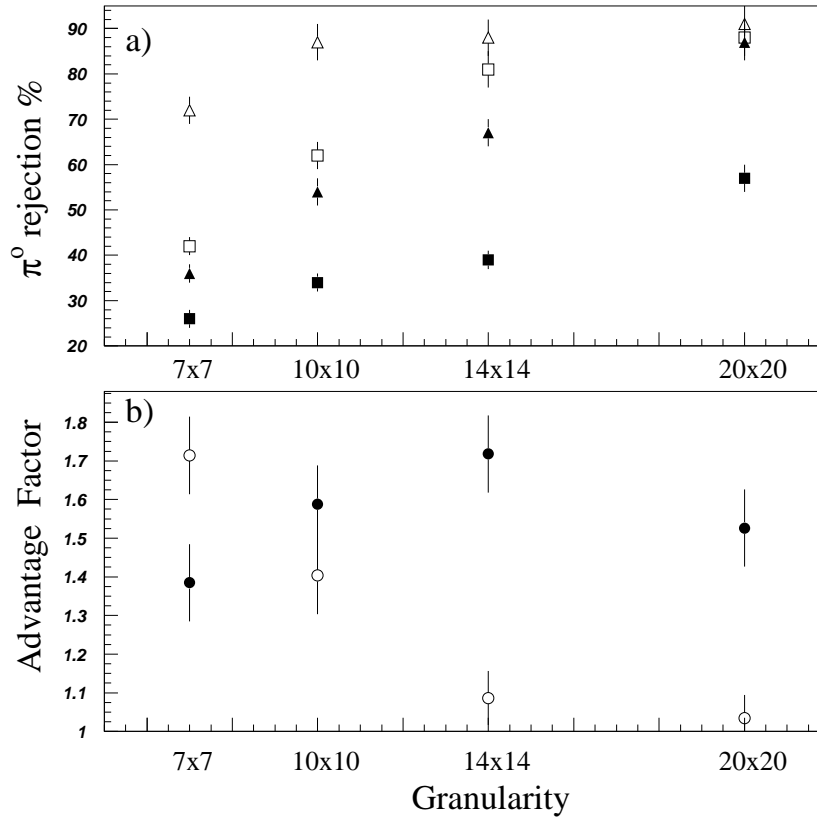


Figure 5: a) The  $\pi^0$  rejection efficiency, as a function of detector granularity, of the SMD-dos ( $\Delta$ ) and a conventional SMD ( $\square$ ) at 50 GeV incident energy; at 100 GeV, SMD-dos ( $\blacktriangle$ ) and a conventional SMD ( $\blacksquare$ ). b) The 'advantage factor' as a function of detector granularity at 50 GeV ( $\circ$ ) and 100 GeV ( $\bullet$ ). The granularity is that of a  $10 \times 10$  cm<sup>2</sup> layer divided into  $n \times n$  square cells.

From the data given in Table 3 it is possible to compare the  $\pi^0$  rejection efficiency performance of the SMD-dos versus the SMD for the same number of channels. For 50 GeV incident energy a SMD-dos detector which has two  $7 \times 7$  layers needs 98 channels in order to read out its 98 cells while a SMD detector of  $10 \times 10$  granularity needs 100 channels. From Table 3 we determine that the SMD-dos is a factor of 1.16 better, 72% vs 62%. A  $10 \times 10$  SMD-dos is better than a  $14 \times 14$  SMD by a factor of 1.07. For 100 GeV incident energy we find that a  $10 \times 10$  SMD-dos is superior to a  $14 \times 14$  SMD by a factor of 1.38. Also a  $14 \times 14$  SMD-dos is a factor of 1.18 better than a  $20 \times 20$  SMD.

Energy = 50GeV					
Number of cells	$\Delta$ [cm]	$\frac{d_{1,2}}{\Delta}$	$\pi^0$ Rejection SMD-dos [%]	$\pi^0$ Rejection SMD [%]	'advantage factor'
7×7	1.43	0.60	72±3	42±2	1.71±0.11
10×10	1.0	0.86	87±4	62±3	1.40±0.09
14×14	0.72	1.20	88±4	81±4	1.09±0.07
20×20	0.50	1.72	91±4	88±4	1.03±0.07
Energy = 100 GeV					
Number of cells	$\Delta$ [cm]	$\frac{d_{1,2}}{\Delta}$	$\pi^0$ Rejection SMD-dos [%]	$\pi^0$ Rejection SMD [%]	'advantage factor'
7×7	1.43	0.30	36±2	26±2	1.38±0.13
10×10	1.0	0.43	54±2	34±3	1.59±0.13
14×14	0.72	0.60	67±2	39±3	1.71±0.12
20×20	0.5	0.86	87±3	57±4	1.52±0.11

Table 3: The  $\pi^0$  rejection efficiencies of the SMD-dos and SMD, the 'advantage factor's, the values of  $\Delta$  and the ratio  $d_{1,2}/\Delta$ , are given for different detector granularities, for 50 and 100 GeV incident energies.

The advantage of using 2 layers which are diagonally off-set with respect to each other as opposed to using a single layer, where the total number of cells of each detector is the same, can be understood as follows: the  $\gamma/\pi^0$  separation power of a granular detector is strongly dependent on the distance of the shower center from an intersection. The success rate of any available  $\gamma/\pi^0$  separation algorithm is higher when the deposited shower energy is distributed among many cells. As previously stated, if all the deposited

energy is collected by a single cell it is impossible to determine the identity of the showering particle. The distance between intersections for a SMD-dos is smaller by a factor of  $1/\sqrt{2}$  than that of a SMD when both detectors have equal number of cells. Therefore, a showering particle incident on a SMD-dos detector will, on the average, have its shower center nearer to an intersection than if it were incident on a SMD detector.

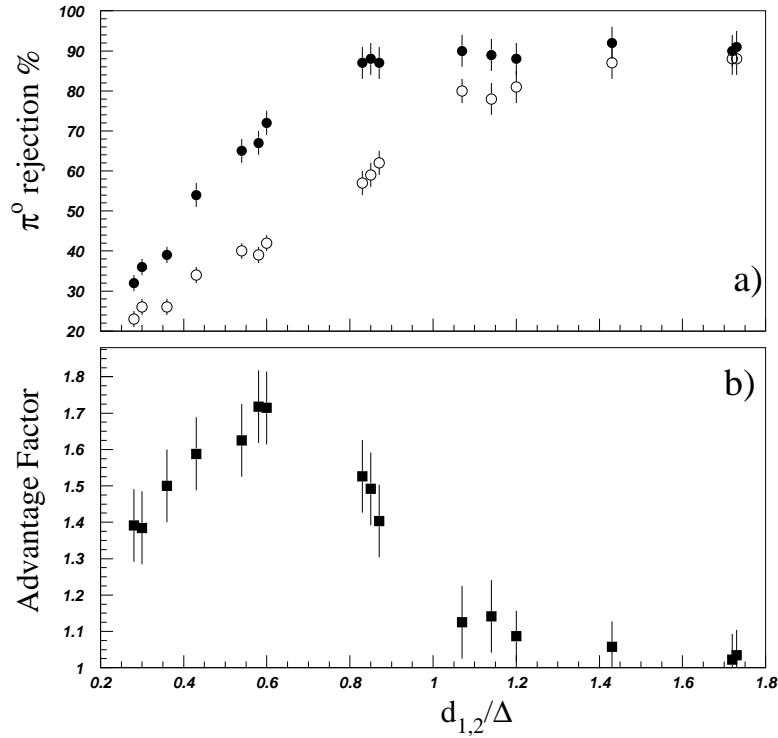


Figure 6: a) The  $\pi^0$  rejection efficiency of the SMD-dos ( $\bullet$ ) and a conventional SMD ( $\circ$ ) as a function of the ratio,  $d_{1,2}/\Delta$ . b) The ‘advantage factor’ as a function of the ratio,  $d_{1,2}/\Delta$ .

The ratio of the 2 variables,  $d_{1,2}$ , the distance between the two  $\gamma$  centers at the position of the SMD-dos or SMD and  $\Delta$ , the length of cell side,  $d_{1,2}/\Delta$ , is a useful a measure of the  $\gamma/\pi^0$  separation difficulty. The  $\gamma/\pi^0$  separation

becomes more difficulty as the ratio  $d_{1,2}/\Delta$  tends to small values while it is significantly easier as the ratio tends to values above 1.0. The behaviour of the  $\pi^0$  rejection efficiency and the ‘advantage factor’ as a function of  $d_{1,2}/\Delta$  are shown in Figure 6. The  $\pi^0$  rejection efficiency, as expected, increases for both the SMD-dos and the SMD as the value of this ratio increases. We notice that the ‘advantage factor’ has an appreciable value only in the range of from  $\sim 0.2$  to  $\sim 1.0$ . That is, when the  $\gamma/\pi^0$  separation is very difficulty, values smaller than  $\sim 0.2$ , than the efficiencies of the SMD-dos and SMD are comparable and likewise when the separation becomes easy, values higher than  $\sim 1.0$ , than again no advantage of SMD-dos over SMD.

If we express,  $d_{1,2}$  in terms of the incident energy,  $E_{inc}$ , mass of the  $\pi^0$  and,  $L$ , distance to SMD-dos or SMD from the interaction point, then we can write the following expression:

$$\frac{d_{1,2}}{\Delta} = \frac{2 \times m_{\pi} \times L}{E_{inc} \times \Delta}.$$

Hence the ratio,  $d_{1,2}/\Delta$ , is a function of 3 independent variables,  $\Delta$ ,  $L$  and  $E_{inc}$ . So for instance if we fix the value of 2 of these variables we can read off from Figure 6 the permissible range of the third variable, for a desired  $\pi^0$  rejection efficiency. Figure 6 can be used, in general, in order to get the  $\pi^0$  rejection efficiency and ‘advantage factor’ for different combinations of the 3 variables not directly studied in this paper. However, it would be prudent to limit the use of these figures to values of the 3 variables which are within a factor of 2 of the ranges explicitly studied in this paper.

## 6 Conclusions

We have designed and extensively studied a new geometry SMD consisting of two layers of scintillator which are diagonally off-set with respect to each other. The layers of scintillator are subdivided into square cells. This geometry has the virtue of increasing substantially the number of intersections per unit area seen by the incoming shower. A comparison of the SMD-dos with a conventional geometry single-layer and mutiple-layer SMD, having the same granularity, shows that the SMD-dos yields higher  $\pi^0$  rejection efficiencies . For 90%  $\gamma$  acceptance the SMD-dos yields  $\pi^0$  rejection efficiencies of  $92 \pm 4$  %,  $87 \pm 4$  % and  $32 \pm 2$  %, respectively, for 30, 50 and 150 GeV incident energies.

We find that the SMD-dos is superior to the SMD, of equal granularity, by an average factor of  $\sim 1.5$  over the 50 to 150 GeV energy range. We also find that the SMD-dos gives better  $\pi^0$  rejection, for the same number of channels, than a SMD. At 100 GeV energy a  $10 \times 10$  cells per layer SMD-dos, which utilizes 200 channels, is a factor of  $\sim 1.4$  better than a  $14 \times 14$  cells, single layer SMD, which utilizes an equal number of channels. The  $\pi^0$  rejection efficiency of the SMD-dos and SMD and the 'advantage factor' are plotted as a function of the ratio,  $d_{1,2}/\Delta$ . With the help of these plots it is possible to investigate the relative importance of the 3 variables,  $\Delta$ ,  $L$  and  $E_{inc}$ , over a range which goes beyond the work presented in this paper. At hadron-hadron colliders the signature of choice for the detection of the Higgs particle, in the mass range of 120 to 160 GeV, is via the decay  $H \rightarrow \gamma\gamma$ . The addition of a SMD-dos to the planned detectors at the LHC would significantly reduce the background to the  $\gamma$  signal coming from prolific  $\pi^0$  production.

## References

- [1] C. Seez, CMS TN/94-288 (Feb 1995).
- [2] S. Shevchenko, CMS TN/94-300.
- [3] G. Apollinari *et al.*, Nucl. Instr. Meth. A324 (1993) 475-481;  
J. Badier *et al.*, Nucl. Instr. Meth. A337 (1994) 314-325;  
B. Aubert *et al.*, Nucl. Instr. Meth. A330 (1993) 405-415.
- [4] J. Grunhaus, S. Kananov and C. Milstene, Nucl. Instr. Meth. A335 (1993) 129-135; Nucl. Instr. Meth. A354 (1995) 368-375.
- [5] T. Muller, 'Proceedings of the SDC Collaboration Meeting at KEK' 26-29 May 1992- KEK- Tsukuba, Japan. Editor H. Iwasaki(KEK), p1463;  
P. Cushman, 'Proceedings of the SDC Collaboration Meeting at KEK' 26-29 May 1992- KEK- Tsukuba, Japan. Editor H. Iwasaki(KEK), p1486.
- [6] D. Acosta *et al.*, Nucl. Instr. Meth. A305 (1991) 55-70.
- [7] P. Bonamy *et al.*, SDC-90-00153, December 1990.

- [8] ATLAS Collaboration, Technical Proposal, Report CERN-LHCC 94-43, December 1994.
- [9] CMS Collaboration, Technical Proposal, Report CERN-LHCC 94-38, December 1994.
- [10] I. Hinchliffe, LBL-34313, June 29, 1993. Workshop on Physics at Current Accelerators and Supercolliders, ANL, June 2-5, 1993;  
Z. Kunszt and F. Zwirner, CERN-TH 6150/91 and ETH-TH 91-7.